THE JOURNAL OF BIOLOGICAL CHEMISTRY
Vol. 276, No. 26, Issue of June 29, pp. 23253–23261, 2001

Printed in U.S.A.

The Giant Protein AHNAK Is a Specific Target for the Calcium- and Zinc-binding S100B Protein

POTENTIAL IMPLICATIONS FOR Ca^{2+} HOMEOSTASIS REGULATION BY S100B*

Received for publication, November 26, 2000, and in revised form, April 18, 2001
Published, JBC Papers in Press, April 18, 2001, DOI 10.1074/jbc.M010655200

Benoit J. Gentil‡, Christian Delphin‡, Gaëlh Ouengue Mbele‡, Jean Christophe Deloulme‡, Myriam Ferro§, Jérôme Garin§, and Jacques Baudier‡¶

From the ‡Département de Biologie Moléculaire et Structurale du Commissariat à l'Energie Atomic, INSERM EPI-0104 and §Laboratoire de Chimie des Proteines DBMS-CP, CEN-G, 38054 Grenoble, France

Transformation of rat embryo fibroblast clone 6 cells by ras and temperature-sensitive p53val^{135} is reverted by ectopic expression of the calcium- and zinc-binding protein S100B. In an attempt to define the molecular basis of the S100B action, we have identified the giant phosphoprotein AHNAK as the major and most specific Ca^{2+}-dependent S100B target protein in rat embryo fibroblast cells. We next characterized AHNAK as a major Ca^{2+}-dependent S100B target protein in the rat glial C6 and human U-87MG astrocytoma cell lines. AHNAK binds to S100B-Sepharose beads and is also recovered in anti-S100B immunoprecipitates in a strict Ca^{2+}- and Zn^{2+}-dependent manner. Using truncated AHNAK fragments, we demonstrated that the domains of AHNAK responsible for interaction with S100B correspond to repeated motifs that characterize the AHNAK molecule. These motifs show no binding to calmodulin or to S100A6 and S100A11. We also provide evidence that the binding of 2 Zn^{2+} equivalents/mol S100B enhances Ca^{2+}-dependent S100B-AHNAK interaction and that the effect of Zn^{2+} relies on Zn^{2+}-dependent regulation of S100B affinity for Ca^{2+}. Taking into consideration that AHNAK is a protein implicated in calcium flux regulation, we propose that the S100B-AHNAK interaction may participate in the S100B-mediated regulation of cellular Ca^{2+} homeostasis.

Calcium is a ubiquitous second messenger that regulates many cellular functions including cell growth, differentiation, and apoptosis (1, 2). EF-hand calcium-binding proteins, such as calmodulin, troponin C, parvalbumin, and S100, are implicated in calcium transduction pathways (3). These proteins bind Ca^{2+} through their EF-hand motifs, and in their Ca^{2+}-bound conformation they interact with secondary effector proteins. S100 proteins constitute one of the largest subfamilies of EF-hand proteins (4). To date, 17 different proteins have been assigned to the S100 protein family. The S100 proteins are small proteins (10 kDa) that are generally expressed in tissue- and cell-specific manners. They show different degrees of homology, ranging from 25% to 55% identity at the amino acid level. *In vivo*, the S100 proteins associate as noncovalent homodimers but may also heterodimerize with other individual S100 species (5–8). Some S100 protein members including S100B, S100A1, S100A3, S100A6, S100A7, and S100A11 are not only calcium-binding proteins but also bind Zn^{2+} ions (9). The interaction of S100B protein with Zn^{2+} may be important in its biological function. Unlike Ca^{2+} binding, Zn^{2+} binding to S100B has a minimal effect on the conformation of the overall protein structure but profoundly increases affinity for calcium (10). An important question related to Zn^{2+} binding to S100 proteins in general is how Zn^{2+} regulates the functions of S100.

S100B is abundant in the brain, where it localizes to astrocytes. This protein has attracted much interest over the past few years because, like other proteins implicated in neurodegeneration (*e.g.* β-amyloid and superoxide dismutase), its gene is located on chromosome 21, which is trisomic in Down's syndrome (11). Overexpression of S100B in the brain of patients with Down's syndrome or Alzheimer's disease (12, 13) and in the brains of patients with AIDS (14) has led to the hypothesis that S100B plays a contributory role in several neuropathologies associated with these diseases. Outside the central nervous system, expression of S100B protein is increased in many tumors (15). In cardiomyocytes, S100B synthesis is induced in response to hypoxia (16) and acts as a negative modulator of the hypertrophic response after myocardial infarction (17). S100B null mice are viable and exhibit no behavioral abnormalities up to 12 month of age (18). On the other hand, astrocytes derived from S100B null mice show abnormal calcium elevation in response to agents that normally induce a transient Ca^{2+} increase (18). These results suggest that S100B plays a role in the maintenance of Ca^{2+} homeostasis within cells. The identification of *in vivo* S100B target proteins is essential for determination of the exact contribution of the S100B-dependent signaling pathways to cellular functions. Several putative S100B target proteins have already been characterized, including cytoplasmic cytoskeletal-associated proteins (19–21); enzymes such as nuclear kinase Ndr (22), retinal membrane-bound guanylate cyclase (23), and fructose 1,6-bisphosphate-aldolase (24); and transcription factors (25, 26). Most of these putative target proteins are also able to interact with the other S100 species and/or calmodulin.

We show here that a major and specific target protein for S100B is the giant phosphoprotein AHNAK. AHNAK/desmoyokin (molecular mass, 700 kDa) is a protein originally identified by Shtivelman *et al.* (27) and Shtivelman and Bishop (28) as a nuclear phosphoprotein repressed in cell lines derived from human neuroblastomas and in several other types of tumors. Subsequently, Hashimoto *et al.* (29) described

* This work was supported by Association pour la Recherche sur le Cancer Grant 5643 and a grant from the Ligue Nationale Contre le Cancer. The costs of publication of this article were defrayed in part by the payment of page charges. This article must therefore be hereby marked "*advertisement*" in accordance with 18 U.S.C. Section 1734 solely to indicate this fact.

¶ To whom correspondence should be addressed: Département de Biologie Moléculaire et Structurale, EPI-0104, Centre d'Etude Nucléaire de Grenoble, 17 rue des Martyrs, 38054 Grenoble Cedex 9, France. Tel: 33-4-38-78-43-28; Fax: 33-4-38-78-58-89; E-mail: jbaudier@cea.fr.

AHNAK/desmoyokin as a desmosomal plaque protein in epithelial tissues. In epithelial cells, AHNAK/desmoyokin is present mainly in the cytoplasm when cells are kept in low Ca^{2+} medium but translocates to the plasma membrane after an increase in extracellular Ca^{2+} concentration or protein kinase C activation (30). More recently, AHNAK has been found in cardiomyocytes associated with L-type calcium channels. In these cells, AHNAK may play a role in cardiac calcium signaling by modulating L-type calcium channels in response to β-adrenergic stimulation (31). A recent report also identified AHNAK as a protein that binds and activates phospholipase C-γ1 in the presence of arachidonic acid to generate inositol trisphosphate and diacylglycerol, two second messengers that control intracellular calcium flux (32). A possible role for AHNAK in S100B-mediated regulation of cell calcium homeostasis is discussed.

MATERIALS AND METHODS

Cell Cultures—REF[1] cells (clone 6) (44) were grown in RPMI 1640-Glutamax (Life Technologies, Inc.) supplemented with 5% fetal calf serum (Life Technologies, Inc.) at 37.5 °C. Glial C6 cells, U87-MG, U373-MG, and HeLa cells were grown in Dulbecco's modified Eagle's medium-Glutamax (Life Technologies, Inc.) supplemented with 10% fetal calf serum (Life Technologies, Inc.) at 37.5 °C.

Antibodies—Purified S100B monoclonal antibody S16 was a generous gift from Dr. M. Takahashi (Skye PharmaTech Inc.). S100B polyclonal antibodies were from DAKO. KIS/AHNAK polyclonal antibodies (28) were obtained from Dr. E. Shtivelman (University of California San Francisco, San Francisco, CA). p53-specific monoclonal antibody PAb421 was purified from hybridoma supernatants by protein A-agarose chromatography. Anti-tubulin was a gift from Dr. L. Paturle and D. Job (CEA-Grenoble). Myc epitope-specific monoclonal antibody 9e10 and MyoD monoclonal antibody 5.8A were from H. Weintraub (Fred Utchinson Cancer Research Center, Seattle, WA).

S100B- and CaM-Sepharose Beads—S100B and CaM were purified from bovine brain to homogeneity (10). S100B- and CaM-Sepharose were prepared by reaction of bovine brain S100B and CaM with CnBr-Sepharose in 20 mM HEPES, pH 7.8, and 0.5 mM $CaCl_2$. Both S100B- and CaM-Sepharose contained 2 mg protein/ml beads. Recombinant human S100B, S100A1, S100A6, and S100A11 were coupled to CnBr-Sepharose (1 mg protein/ml beads) as described above.

Bacterial Expression Plasmids—The bacterial expression plasmid for the production of His-tagged M2-DY (AHNAK amino acids 2589–3059) was constructed by cloning an *Eco*RV/*Hin*dIII fragment from Z83 (27) into *Eco*RV/*Hin*dIII sites of pet32b (Novagen). For His-tagged M3-DY (AHNAK amino acids 3730–4188) expression in *Escherichia coli*, the corresponding *Ssp*I DNA fragment from Z80 (27) was cloned into *Eco*RV site of pet32a (Novagen). His-tagged U1-DY (AHNAK amino acids 3730–3878) and His-tagged U2-DY (AHNAK amino acids 3730–3972) expression plasmids were obtained by deleting the carboxyl-terminal part of the AHNAK fragment of M3-DY. M3-DY expression vector was digested by *Bsp*MI/*Xho*I or *Aat*II/*Xho*I for the production of U1-DY or U2-DY expression vector, respectively, blunted, and then self-ligated.

Recombinant Protein Expression and Purification—Recombinant protein expression was carried out in *E. coli* strain AD494(DE3)pLYsS (Novagen). Bacteria were grown to $A_{600} = 0.6$ in 100 ml of Luria-Bertani broth medium supplemented with 15 μg/ml kanamycin, 34 μg/ml chloramphenicol, 40 μg/ml leucine, and 50 μg/ml carbemicillin. Protein expression was induced with 1 mM isopropyl-1-thio-β-D-galactopyranoside for 2 h. Bacteria were harvested and resuspended in 2 ml of lysis buffer (30 mM Tris-HCl, pH 7.4, 150 mM NaCl, 0.3% Triton X-100, 1 mM β-mercaptoethanol, 1 mg/ml lysozyme, and 2 μg/ml of each protease inhibitor (leupeptin, aprotinin, pepstatin, and AEBSF)). After one freeze/thaw cycle, bacterial lysates were cleared (100,000 × *g* for 20 min) and kept on ice or stored at −20 °C. His-tagged M3-DY, U2-DY, and U1-DY were purified by Ni^{3+} affinity chromatography.

S100B- and CaM-binding Assays—For binding assays using recombinant AHNAK fragments expressed in rabbit reticulocytes (TNTquick; Promega), 20 μl of reaction lysates were diluted in 500 μl of TTBS supplemented with either 5 mM EDTA and 5 mM EGTA or 0.3 mM $CaCl_2$ and 10 μM $ZnSO_4$ and mixed with 20 μl of affinity beads equilibrated in the same buffers. After mixing at 4 °C for 10 min, the beads were spun down, and the supernatant was removed. The beads were washed three times with the binding buffers and boiled in SDS-sample buffer. For binding assays using recombinant AHNAK fragments expressed in bacteria, soluble extracts (50 μl) were diluted in 500 μl of TTBS supplemented with either 5 mM EDTA and 5 mM EGTA or 0.3 mM $CaCl_2$ and 10 μM $ZnSO_4$ and treated as described above. For binding assays using crude cell extracts, cells were first labeled in methionine-free minimum Eagle's medium, 10% fetal calf serum, supplemented with [^{35}S]methionine/[^{35}S]cysteine mix (50 μCi/ml) for 8 h. Cells were lysed in TTBS buffer supplemented with protease inhibitors (leupeptin, aprotinin, pepstatin, AEBSF, *N*-acetyl-Leu-Leu-norleucinal, and *N*-acetyl-Leu-Leu-methioninal; 10 μg/ml each) and centrifuged for 10 min at 14,000 × *g*. The lysates were precleared by incubation for 10 min with 50 μl of protein A-Sepharose. Aliquots (500 μl) of precleared supernatant were mixed with 500 μl of TTBS supplemented with either 5 mM EDTA and 5 mM EGTA or 0.3 mM $CaCl_2$ and 10 μM $ZnSO_4$ and mixed with 20 μl of affinity beads equilibrated in the same buffers. After mixing at 4 °C for 10 min, the beads were spun down, and the supernatant was removed. The beads were washed three times with the binding buffers. At the last wash, the beads were transferred to new Eppendorf tubes and boiled in SDS-sample buffer.

Co-immunoprecipitations—For co-immunoprecipitation of AHNAK and S100B, NIH-3T3 cells in 100-mm dishes were first transfected with control plasmid or S100B plasmid (4 μg) using FuGENE™ reagent (12 μl) as recommended by the manufacturer (Roche). Cells were lysed after 36 h. For co-immunoprecipitation of p53 and AHNAK, confluent REF cells were labeled in methionine-free minimum Eagle's medium, 5% fetal calf serum, supplemented with [^{35}S]methionine/[^{35}S]cysteine mix (100 μCi/ml) for 6 h. NIH-3T3 and REF cells were lysed in TTBS buffer supplemented with protease inhibitors (leupeptin, aprotinin, pepstatin, AEBSF, *N*-acetyl-Leu-Leu-norleucinal, and *N*-acetyl-Leu-Leu-methioninal; 10 μg/ml each). The lysates were precleared by a 10-min centrifugation at 14,000 × *g*, and the supernatant was further incubated for 15 min with 50 μl of protein A-Sepharose. Aliquots (500 μl) of precleared supernatant were mixed with 500 μl of TTBS supplemented with either 5 mM EDTA and 5 mM EGTA or 0.3 mM $CaCl_2$ and 10 μM $ZnS0_4$ and mixed with appropriate antibodies (5 μg) plus 20 μl of protein A-Sepharose equilibrated in the same buffers. After mixing at 4 °C for 15 min, the beads were centrifuged briefly (5 s, 13,000 rpm), and the supernatant was removed. The beads were washed three times with the binding buffers. At the last wash, the beads were transferred to new Eppendorf tubes and boiled in SDS-sample buffer.

Mass Spectrometric Analysis and Protein Identification—The protein bands were excised from Coomassie Blue-stained gels and washed with 50% acetonitrile. Gel pieces were dried in a vacuum centrifuge and reswollen in 20 μl of 25 mM NH_4HCO_3 containing 0.5 μg of trypsin (sequencing grade; Promega). After 4 h of incubation at 37 °C, a 0.5 μl aliquot was removed for MALDI time of flight analysis and spotted onto the MALDI sample probe on top of a dried, 0.5 μl mixture of 4:3 saturated α-cyano-4-hydroxy-*trans*-cinnamic acid in acetone/10 mg/ml nitrocellulose in acetone/isopropanol 1:1. Samples were rinsed by placing a 5 μl volume of 0.1% trifluoroacetic acid on the matrix surface after the analyte solution had dried completely. After 2 min, the liquid was blown off by pressurized air. MALDI mass spectra of peptide mixtures were obtained using a Bruker Biflex mass spectrometer (Bruker-Franzen Analityk, Bremen, Germany). Internal calibration was applied to each spectrum using trypsin autodigestion peptides (MH+ 842.50, MH+ 1045.55, and MH+ 2211.11). Protein identification was confirmed by tandem mass spectrometry experiments. After in-gel tryptic digestion, the gel pieces were extracted with 5% formic acid solution and then extracted with acetonitrile. The extracts were combined with the original digest, and the sample was evaporated to dryness in a vacuum centrifuge. The residues were dissolved in 0.1% formic acid and desalted using a Zip Tip (Millipore). Elution of the peptides was performed with 5–10 μl of 50% acetonitrile/0.1% formic acid solution. The peptide solution was introduced into a glass capillary (Protana) for nanoelectrospray ionization. Tandem mass spectrometry experiments were carried out on a quadrupole time of flight hybrid mass spectrometer (Micromass, Altrincham, United Kingdom) to obtain sequence information. Collision-induced dissociation of selected precursor ions was performed using argon as the collision gas and with collision energies of 40–60 eV. Protein identification was achieved using both MALDI peptide mass fingerprints and tandem mass spectrometry sequence information. Mass spectrometric data were compared with known sequences using the programs MS-Fit and MS-Edman from the University of California San Francisco.

[1] The abbreviations used are: REF, rat embryo fibroblast; CaM, calmodulin; TTBS, 40 mM Tris-HCl, pH 7.5, 150 mM NaCl, and 0.3% Triton X-100; MALDI, matrix-assisted lazer desorption ionization; PAGE, polyacrylamide gel electrophoresis.

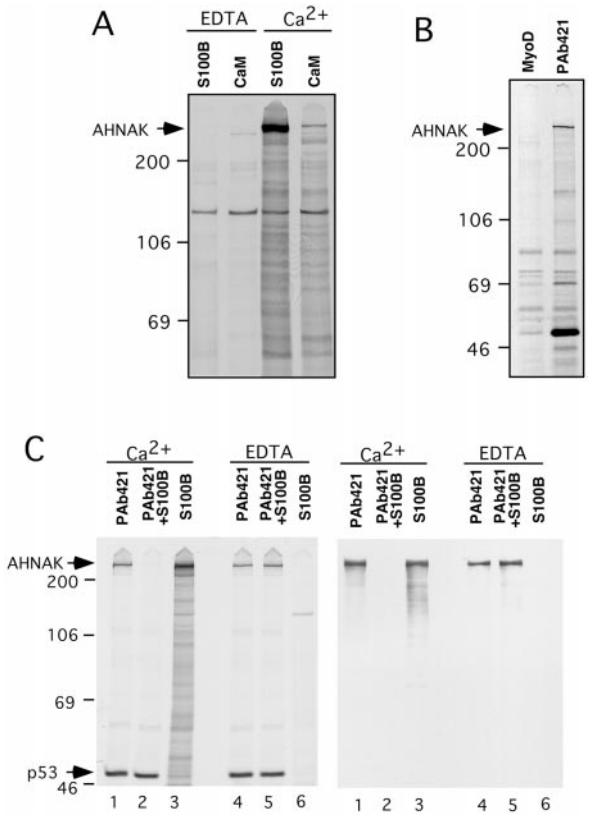

FIG. 1. **AHNAK in REF clone 6 cells interacts with S100B.** *A,* comparison of [^{35}S]methionine-labeled proteins in REF cell extracts that interact with S100B-Sepharose (*S100B*) or CaM-Sepharose (*CaM*) beads in the absence (*EDTA*) or presence of calcium (Ca^{2+}). The bound proteins were resolved on 5% SDS-PAGE without stacking gel and autoradiographed. *B,* analysis of [^{35}S]methionine-labeled proteins in REF cell extracts that co-precipitate with p53val^{135}. Cell extracts were immunoprecipitated with either MyoD monoclonal antibody 5.8A or p53-specific monoclonal antibody PAb421 as indicated. Immunoprecipitates were resolved by 7.5% SDS-PAGE and autoradiographed. *C,* S100B prevents co-precipitation of AHNAK with p53val^{135}. *Left panel,* [^{35}S]methionine-labeled proteins in REF cell extracts were incubated with p53 monoclonal antibody PAb421 coupled to Sepharose in the absence (*lanes 1* and *4*) or presence of 5 μM purified S100B (*lanes 2* and *5*). Identical extracts were incubated with S100B-Sepharose in the presence (*lanes 3*) or absence of calcium (*lanes 6*). The bound proteins were electrophoresed on 7.5% SDS-PAGE gels and autoradiographed. *Right panel,* REF cells extracts were treated as described for the *left panel*. Proteins were electrophoresed on 5% SDS-PAGE and detected by Western blot analysis using KIS/AHNAK antibodies.

Real-time Surface Plasmon Resonance Recording—Real-time binding experiments were performed on a BIAcore biosensor system (Pharmacia Biosensor AB, Uppsala, Sweden). All experiments were performed at 25 °C. AHNAK peptides in 10 mM sodium acetate, pH 3.5, were coupled directly through their amino groups to the sensor surface activated by *N*-hydroxy-succinimide and *N*-ethyl-*N*′-(dimethylaminopropyl)carbodiimide according to the manufacturer's instructions. The remaining reactive groups were then inactivated with 1 mM ethanolamine. For control experiments, the sensor surface was treated as described above in the absence of peptide or coupled to His-tagged importin α1. All interaction experiments were done using a running buffer containing 20 mM Tris-HCl, pH 7.5, and 150 mM NaCl in the absence or presence of $CaCl_2$ as indicated. Between injections, the sensor chip was washed with a buffer containing 20 mM Tris-HCl, pH 7.5, 120 mM NaCl, and 2 mM EDTA and equilibrated with the appropriate running buffer. For Zn^{2+}-dependent binding experiments, the S100B protein was incubated with $ZnS0_4$ before injection on the sensor chip. Sensorgrams were analyzed using the BIAevaluation 3.0 program (Pharmacia Biosensor AB).

RESULTS

Identification of the Giant Protein AHNAK as a Target Protein for S100B in Fibroblastic Cell Lines—Ectopic expression of the calcium- and zinc-binding S100B protein in mouse embryo fibroblasts and REFs expressing the temperature-sensitive p53val^{135} mutant cooperates with Ca^{2+} to promote nuclear accumulation of the wild-type p53val^{135} conformational species and rescue wild-type p53 functions at the nonpermissive temperature (33, 34). To begin to characterize the mechanism behind this effect, we chose to characterize Ca^{2+}-dependent S100B target proteins in REF clone 6 cells. REF cells were metabolically labeled with [^{35}S]methionine, after which protein extracts were incubated with S100-Sepharose beads in the absence or presence of Ca^{2+}/Zn^{2+}. To control for specificity of protein interactions, the pattern of protein binding was compared with that of CaM-Sepharose (Fig. 1*A*). The most abundant and specific calcium-dependent S100B target protein in REF cells is a large protein heavily labeled with [^{35}S]methionine that migrates at the top of the gel (Fig. 1*A*).

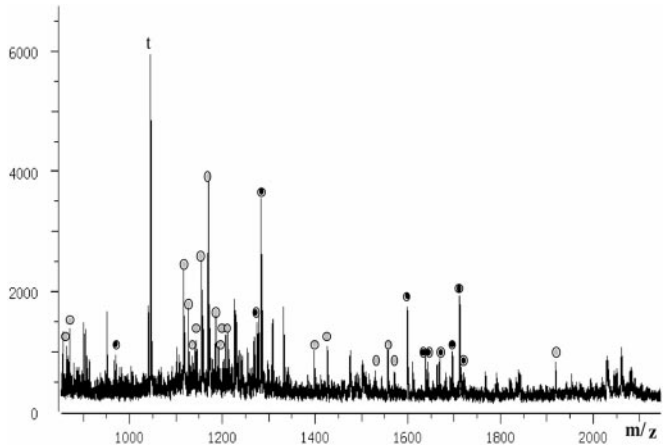

FIG. 2. **Identification of AHNAK by mass spectrometry.** Nanoelectrospray mass spectral analysis was performed on the high molecular weight specific S100B target protein isolated from human HeLa cells as described under "Materials and Methods." Positive-ion mass spectrum of the tryptic peptide mixture obtained from in-gel digestion and microcolumn desalting is shown. The molecular weight of peptide ions indicated with *gray-filled circles* matched tryptic peptides from AHNAK. Peptides indicated with *black-filled circles* were sequenced by tandem mass spectrometry and found to match tryptic peptides from AHNAK. *t,* tryptic peptide from trypsin.

The corresponding human protein from HeLa cell extract was next isolated by Ca^{2+}-dependent interaction with S100B-Sepharose beads and further characterized by mass spectrometry. Protein identification was achieved using both MALDI peptide mass fingerprints and tandem mass spectrometry sequence information (Fig. 2). Results revealed that the large molecular mass protein corresponds to the human protein AHNAK (27).

A physical Ca^{2+}-dependent interaction between S100B and AHNAK was also demonstrated by exploiting the observation that AHNAK co-immunoprecipitates with the anti-p53 monoclonal antibody PAb421 from clone 6 cell extracts (Fig. 1*B* and Fig. 1*C, lanes 1* and *4*). AHNAK is not precipitated by the control monoclonal anti-MyoD antibody, showing that AHNAK co-immunoprecipitation with PAb421 is specific (Fig. 1*B*). If clone 6 cell extracts are supplemented with purified S100B (5 μM) before immunoprecipitation with PAb421, S100B prevents co-precipitation of AHNAK only when calcium is present (Fig. 1*C,* compare *lanes 1* and *2*). In the absence of calcium, AHNAK is unable to interact with S100B (*lanes 6*), and S100B does not dissociate AHNAK from PAb421 immunoprecipitates (Fig. 1*C,* compare *lanes 4* and *5*). S100B does not antagonize p53val^{135} immunoprecipitation by PAb421 (Fig. 1*C,* compare *lanes 1* and *4* with *lanes 2* and *5*), confirming that the dissociation of AHNAK from PAb421 immunoprecipitate results from direct interaction between S100B and AHNAK.

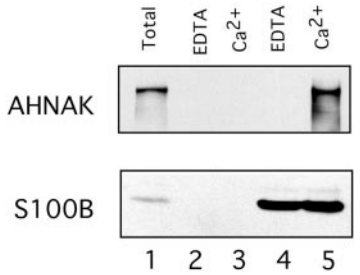

FIG. 3. **Co-immunoprecipitation of AHNAK with S100B.** NIH-3T3 cells were transfected with an expression plasmid containing the S100B gene (*lanes 1, 4,* and *5*) or empty vector alone (*lanes 2* and *3*). After 36 h, cells were lysed in detergent-containing buffer and incubated with protein A-Sepharose and S100B monoclonal antibody S16 in the absence (*lanes 2* and *4*) or presence of calcium (*lanes 3* and *5*). Immunoprecipitates were either electrophoresed on 5% SDS-PAGE and analyzed for AHNAK by Western blot or electrophoresed on 11% SDS-Tricine PAGE followed by Western blot analysis for S100B. *Lane 1* corresponds to total extract of NIH-3T3 cells transfected with the S100B gene.

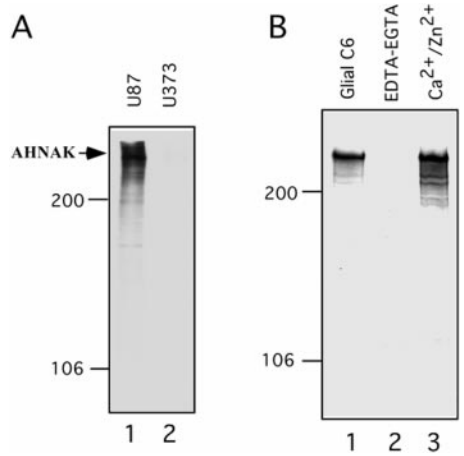

FIG. 4. **AHNAK is present in glial cells.** *A,* AHNAK is present in the human astrocytoma cell line U87-MG (*lane 1*) but not in U373-MG cells (*lane 2*). Cell extracts were analyzed by Western blot using KIS/AHNAK polyclonal antibodies. *B,* characterization of AHNAK as a calcium-dependent target for S100B in rat glial C6 cells. Proteins from total glial C6 extract (*lane 1*) and proteins that bound to S100B-Sepharose in the absence (*lane 2*) or presence of calcium (*lane 3*) were analyzed by Western blot using KIS/AHNAK polyclonal antibodies.

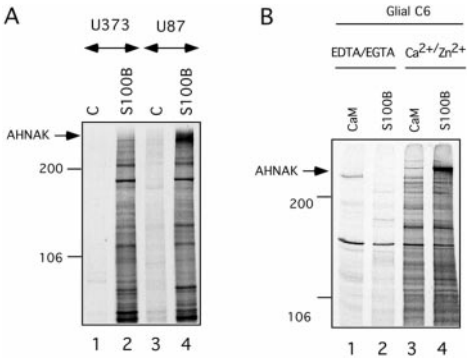

FIG. 5. **AHNAK is a major and specific calcium-dependent target for S100B in glial cell lines C6 and U87-MG.** *A,* comparison of soluble proteins in human astrocytoma U373-MG (*lanes 1* and *2*) and U87-MG cells (*lanes 3* and *4*) that bound to Sepharose (*lanes 1* and *3*) or to S100B-Sepharose (*lanes 2* and *4*) in the presence of calcium. *B,* comparison of soluble proteins in glial C6 extract that interact with CaM-Sepharose (*lanes 1* and *3*) or S100B-Sepharose (*lanes 2* and *4*) in the absence (*lanes 1* and *2*) or presence of calcium (*lanes 3* and *4*). In *A* and *B,* cells were metabolically labeled with [^{35}S]methionine for 8 h before lysis. Cell extracts (1 ml) were incubated with 20 μl of either Sepharose or Sepharose coupled to CaM or S100B in the absence or presence of calcium. The bound proteins were electrophoresed on 5% SDS-PAGE and visualized by autoradiography.

Finally, we confirmed a strict Ca^{2+}-dependent interaction between S100B and AHNAK by co-immunoprecipitation (Fig. 3). NIH-3T3 cells were transfected with an expression vector containing S100B cDNA, and complex formation was assayed by co-immunoprecipitation. AHNAK co-immunoprecipitates with S100B from cell lysates containing Ca^{2+} and Zn^{2+} (Fig. 3, *lane 5*) but not in the presence of EGTA/EDTA (Fig. 3, *lane 4*). The co-immunoprecipitation of AHNAK with S100B was specific because it was not observed in cells transfected with empty vector (Fig. 3, *lanes 2* and *3*).

Characterization of AHNAK as a Major Calcium-dependent S100B Target in Glial Cells—In humans, the S100B protein is abundant in the adult central nervous system, where it accumulates in glial cells. We therefore evaluated the presence of AHNAK in two human astrocytoma cell lines (U373-MG and U87-MG) (Fig. 4*A*) and one rat glioma cell line (C6) (Fig. 4*B*). Western blot analysis of crude cell extracts revealed that only human U-87-MG cells (Fig. 4*A, lane 1*) and rat C6 cells (Fig. 4*B, lane 1*) show strong AHNAK immunoreactivity. AHNAK was absent in the human astrocytoma cell line U-373-MG (Fig. 4*A, lane 2*; see also Fig. 5*A*). Western blot analysis (Fig. 4*B*) as well as affinity batch interaction studies using [^{35}S]methionine-labeled cells (Fig. 5) confirmed the strict calcium-dependent interaction of the AHNAK protein in U-87-MG cells and glial C6 cells with S100B-Sepharose beads. Note, here again, that most of the proteins that bound to S100B-Sepharose also bound to CaM-Sepharose and that AHNAK is the only protein that specifically bound to S100B-Sepharose beads in a strict Ca^{2+}/Zn^{2+}-dependent manner (Fig. 5*B, lanes 3* and *4*).

Identification of the S100B-binding Region of AHNAK—A three-domain structure was predicted for AHNAK in which the amino- and carboxyl-terminal ends of the protein flank a large internal domain (Fig. 6*A*). The internal domain is composed of 30 repeated motifs, each of which is 128 residues long (27). The 128-residue motifs are, on average, ~80% identical to each other with respect to amino acid sequence. The 128-residue repeat is characterized by underlying heptad repeats that are also found in the first portion of the carboxyl terminus. To investigate which domains of AHNAK are responsible for specific binding to S100B, the amino terminus (residues 1–251, N-DY), four complete repeating units of the central domain (residues 820–1330, M1-DY), and the carboxyl-terminal 1002 amino acids (C-DY) tagged with a Myc epitope were translated *in vitro* using rabbit reticulocyte lysates. The interaction of the Myc-tagged AHNAK domains with anti-Myc and with S100B- or CaM-Sepharose was evaluated. The amino terminus was unable to bind to S100B- or CaM-Sepharose (Fig. 6*B*). The carboxyl terminus was found to bind to S100B-Sepharose and, to a much lesser extent, to CaM-Sepharose in a strictly Ca^{2+}/Zn^{2+}-dependent manner (Fig. 6*C*). The M1-DY domain showed absolutely no binding to CaM-Sepharose but interacted strongly with the S100B-Sepharose in a Ca^{2+}/Zn^{2+}-dependent manner (Fig. 6*C*). The specificity of the interaction of S100B with the M1-DY domain was confirmed by comparison with three other S100 proteins, S100A1, S100A6, and S100A11 (Fig. 6*D*). Only S100A1-Sepharose showed a faint Ca^{2+}-dependent interaction with M1-DY, albeit with a much lower avidity than S100B.

To confirm the contribution of the AHNAK repeat units to S100B binding, we next analyzed the interaction of two bacterial recombinant fusion AHNAK domains containing different repeating units from the central domain (M2-DY and M3-DY, see Fig. 6*A*) with S100B- and CaM-Sepharose. Both M2-DY and

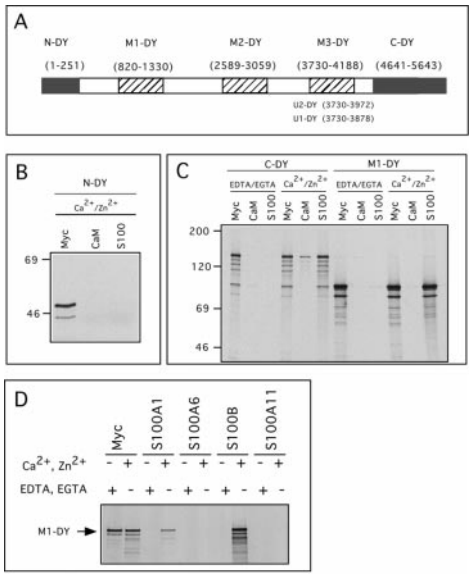

FIG. 6. **Identification of the S100B-binding domain of AHNAK.** *A,* schematic diagram of AHNAK showing the amino terminus (*N-DY*), central repeating units (*M1-DY, M2-DY,* and *M3-DY*), and carboxyl terminus (*C-DY*) AHNAK fragments used in this study. *Numbers* refer to the amino acid sequence of AHNAK domains. *B* and *C,* different Myc-tagged AHNAK domains corresponding to N-DY (*B*) and C-DY and M1-DY (*C*) were translated with rabbit reticulocytes. Equal amounts of the translation reaction (20 μl) were immunoprecipitated with monoclonal antibody against Myc-tag (*Myc*) or incubated with 20 μl of bovine brain CaM-Sepharose (*CaM*) or S100B-Sepharose (*S100*) in 1 ml of buffer supplemented with 5 mM EDTA/EGTA (*EDTA/EGTA*) or 0.2 mM Ca^{2+} + 10 μM Zn^{2+} (*Ca^{2+}/Zn^{2+}*) as indicated. Bound proteins were electrophoresed on 8% SDS-PAGE gels and visualized by autoradiography. *D,* comparison between human recombinant S100-Sepharose proteins (1 mg/ml Sepharose) in binding Myc-tagged M1-DY domain translated in rabbit reticulocyte lysates. Incubation buffer contained 5 mM EDTA/EGTA or 0.2 mM Ca^{2+} + 10 μM Zn^{2+} as indicated.

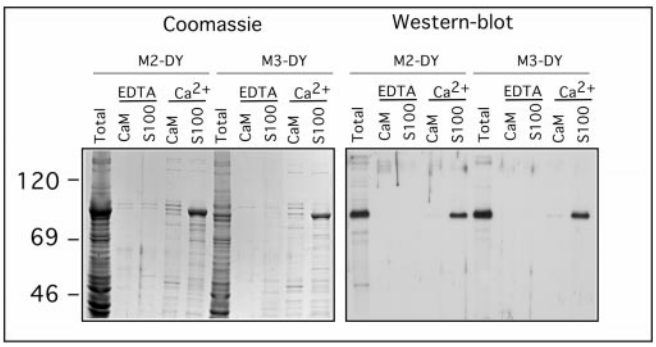

FIG. 7. **Binding of M2-DY and M3-DY to S100B.** AHNAK domains corresponding to M2-DY and M3-DY were expressed as recombinant proteins in bacteria. Calcium-dependent binding of the soluble bacterial proteins (*Total*) to CaM-Sepharose (*CaM*) or S100B-Sepharose (*S100*) was compared. Proteins were electrophoresed on 8% SDS-PAGE gels and revealed either by Coomassie Blue staining (*left panel*) or by Western blot analysis using KIS/AHNAK antibodies (*right panel*).

M3-DY specifically bound to S100B in a calcium-dependent manner but did not bind to CaM (Fig. 7).

S100B Binding to AHNAK Repeated Units—The interaction between S100B and AHNAK repeat units was next analyzed using surface plasmon resonance detection. His-tagged recombinant AHNAK peptides comprising three-repeat units (M3-DY, residues 3730–4188), two repeat units (U2-DY, residues 3730–3972), and one repeat unit (U1-DY, residues 3730–3878) were purified to homogeneity (Fig. 8*A, inset*) and separately coupled to the biosensor chip. Note that purified U1-DY shows two protein bands in SDS-PAGE. These two protein bands are recognized by KIS/AHNAK antibodies (data not shown). The lower band is most likely a proteolytic product of the full-length U1-DY.

Fig. 8*A* shows a typical sensorgram representing the real-time interaction between purified Ca^{2+}/Zn^{2+}-bound S100B and M3-DY peptide. In these experiments, S100B was injected onto the biosensor chip with 2 Zn^{2+} equivalents/mol S100B monomer and 0.1 mM $CaCl_2$, and the sensor chip was then washed with Ca^{2+}-containing buffer in the absence of Zn^{2+}. The Ca^{2+}/Zn^{2+}-dependent interaction of S100B with M3-DY is completely reversed by the addition of EDTA to the buffer. The reversibility of the interaction allows recycling of the biosensor chip with EDTA-containing buffer and permits a dose-dependent titration of the interaction with the same biosensor chip.

Fig. 8*B* shows the kinetics of the interaction between S100B at different concentrations with U2-DY peptide. The specificity of the interaction of S100B with U2-DY peptide is also assessed by comparison with bovine brain CaM and human recombinant S100A1, S100A6, and S100A11 (Fig. 8*B, inset*). Neither CaM, S100A1, S100A6, nor S100A11 showed interaction with the AHNAK peptide-coated sensor chip.

As shown in the *inset* in Fig. 8*C,* purified U1-DY peptides bind to S100B-Sepharose beads in a strict Ca^{2+}/Zn^{2+}-dependent manner. Fig. 8*C* shows the kinetics of the interaction between S100B at different concentrations with U1-DY peptides. The best fit of the curve obtained with one repeat unit and 250 nM S100B was obtained with a 1:1 binding model and an estimated K_d of 50 nM. Taken together, these data indicate that one AHNAK repeat is sufficient for S100B binding.

Ca^{2+} and Zn^{2+} Dependence of S100B Binding to AHNAK Repeated Units—We next investigated the respective contributions of Zn^{2+} and Ca^{2+} to the S100B-AHNAK interaction. To begin, we studied the effect of Zn^{2+} alone on S100B binding to U2-DY peptide (Fig. 9*A*). In those experiments, S100B was incubated with 2 Zn^{2+} equivalents/mol S100B monomer before injection onto the biosensor chip. There was no binding of Zn^{2+}-S100B to AHNAK peptide in Ca^{2+}-free buffer. We confirmed this observation by analyzing the interaction of ^{35}S-labeled Myc-tagged M1-DY AHNAK domains with S100B-Sepharose beads (Fig. 9*B*). Zn^{2+} alone does not promote M1-DY binding to S100B-Sepharose. We next studied the effect of Zn^{2+} on Ca^{2+}-dependent binding of S100B to AHNAK peptides. In the absence of Zn^{2+}, only a faint interaction between S100B and U2-DY peptide coupled to the biosensor chip was observed at 100 μM $CaCl_2$ (Fig. 9*A*). Calcium titration of the interaction between Myc-tagged M1-DY AHNAK domains and S100B-Sepharose beads confirmed that 100 μM $CaCl_2$ is not sufficient for maximum interaction (Fig. 9*B*). If S100B is incubated with 2 Zn^{2+} equivalents/mol S100B monomer before injection onto the biosensor chip, the intensity of the interaction signal between S100B and the U2-DY peptide increases (Fig. 9*A*). In the presence of Zn^{2+}, calcium titration of the interaction between Myc-tagged M1-DY AHNAK domains and S100B-Sepharose beads is shifted to lower concentrations, with maximum binding at 50 μM $CaCl_2$ (Fig. 9*B*). Such a shift is compatible with the positive effect of Zn^{2+} on S100B affinity for calcium (10) and is in agreement with previous determinations of the *in vitro* binding affinity of S100B for Ca^{2+} under the same experimental conditions (10). The effect of Zn^{2+} on Ca^{2+}-dependent interaction of S100B with U2-DY peptide is maximal with the addition of 2 Zn^{2+} equivalents/mol S100B and is decreased at higher Zn^{2+}:S100B molar ratios (Fig. 9*C*). This observation is consistent with previous reports showing that binding of 2 Zn^{2+} equivalents/mol S100B has the pronounced effect of increasing calcium affinity in S100B, whereas this effect is reversed at higher molar ratios (10).

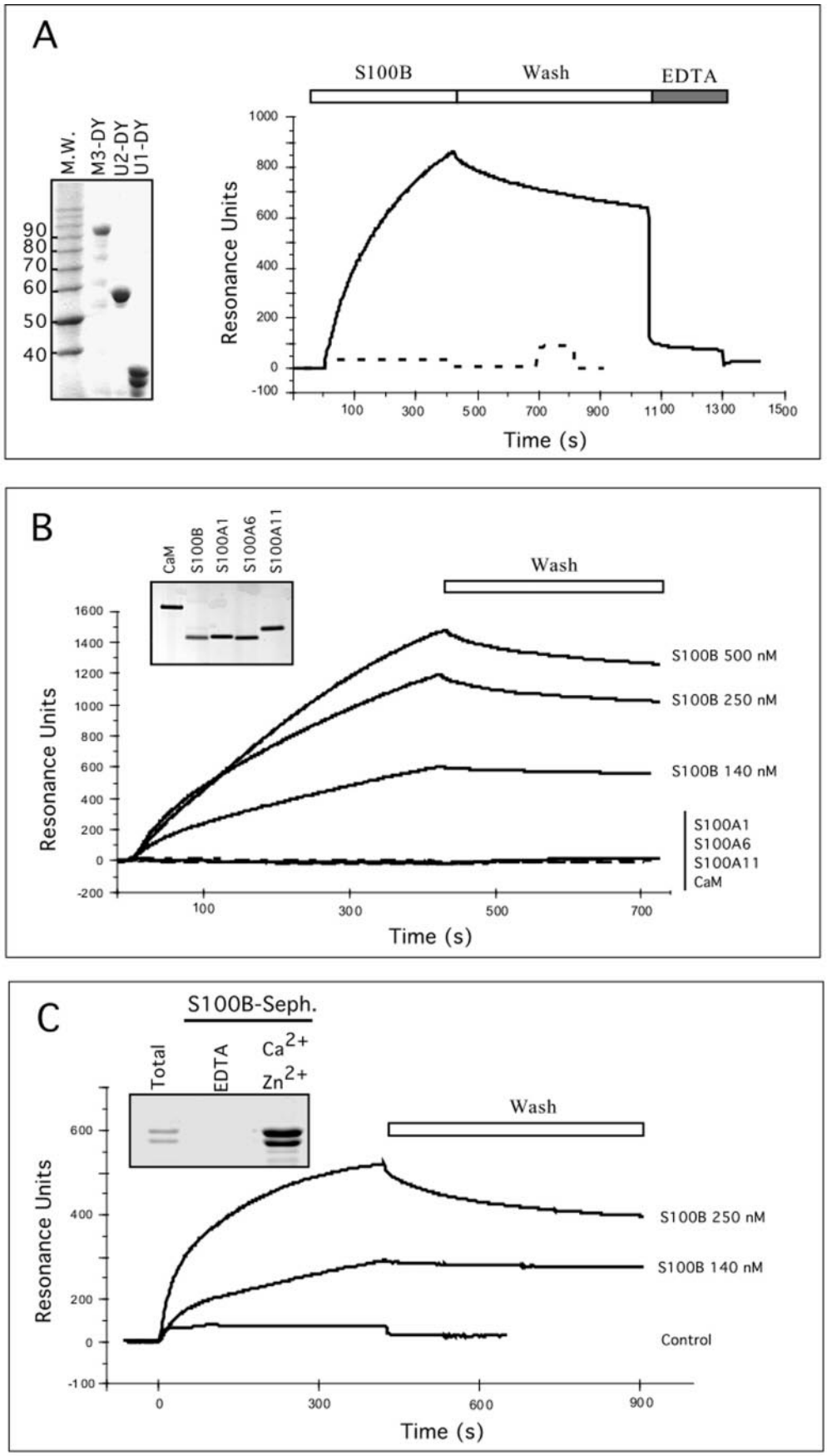

FIG. 8. **Characterization of the interaction of purified S100B with AHNAK peptides using surface plasmon resonance detection.** *A,* His-tagged M3-DY peptide and His-tagged importin α1 (*dashed line*), which was used as a control, were covalently immobilized on the sensor surface as described under "Materials and Methods." Running buffer contains 20 mM Tris-HCl, pH 7.5, 150 mM NaCl, and 0.1 mM $CaCl_2$. Recombinant human S100B (140 nM) in the presence of 280 nM $ZnSO_4$ was injected (*solid line*). At the end of the injection, the sensor surface was washed with running buffer and then washed with a buffer containing 2 mM EDTA. *Inset* shows SDS-PAGE and Coomassie Blue staining of the

DISCUSSION

Identification of *in vivo* S100B target proteins represents a first step toward understanding the exact contribution of the S100B protein to calcium-dependent signaling pathways. In this study, we have presented data that suggest that the giant protein AHNAK is a specific calcium-dependent S100B target. AHNAK is the major protein that binds to S100B-Sepharose beads from REF clone 6 cell extracts and from two different astrocyte cell lines. A specific Ca^{2+}/Zn^{2+}-dependent interaction of AHNAK with S100B was confirmed by co-immunoprecipitation (Fig. 3). An overlapping specificity of S100B and CaM for interaction with target proteins, peptides, and drugs is often observed (19, 22, 35). Hence, most of the proteins in crude cell extracts that bind S100B-Sepharose beads also bind to CaM. AHNAK is the only protein identified to date that demonstrates a strict Ca^{2+}/Zn^{2+}-dependent interaction with S100B and absolutely no binding to CaM (Figs. 1*A* and 5*B*). That specificity of interaction has been confirmed using different AHNAK peptide domains. The same specificity of the S100B-AHNAK interaction was further confirmed with the finding that other S100 molecules do not bind AHNAK under similar conditions (Figs. 6*D* and 8*B*). S100B may thus represent a specific AHNAK regulator protein.

AHNAK is a protein of an unusually large size. The interaction of small EF-hand calcium binding proteins with giant proteins has a precedent in the literature. Two giant protein kinases, titin (3000 kDa) and twitchin (750 kDa), interact with Ca^{2+}-CaM and Ca^{2+}/Zn^{2+}-S100A1, respectively (36). However, no kinase domain is predicted based on AHNAK structure. Another distinctive feature of the AHNAK protein is the repeated 128-residue motifs that characterize the middle portion and the carboxyl-terminal domain of the protein (27). Inspection of the 128-residue repeat revealed an underlying heptad repeat with the motif $\psi\pm\psi P\pm\psi\pm$, where ψ is a hydrophobic residue, $\pm$ is a hydrophilic residue, and P is proline (27). Internal domain peptide (M1-DY, M2-DY, and M3-DY) and the carboxyl-terminal end (C-DY) of the protein display similar specific calcium-dependent binding to S100B (Figs. 6*C* and 7). It is thus likely that the repeated units represent structural elements involved in S100B binding. The interaction between S100B and AHNAK repeat units was confirmed using surface plasmon resonance detection (Fig. 8). The experiments shown in Fig. 8*C* indicate that one repeat unit is sufficient for binding S100B. Although CaM and other S100 proteins species are unable to interact with the internal domain peptides of AHNAK (M1-DY, M2-DY and M3-DY), a faint interaction of the carboxyl terminus of AHNAK (C-DY) with CaM is nevertheless observed (Fig. 6*C*). The extreme carboxyl terminus of AHNAK is characterized by a high proportion of basic and hydrophobic amino acids, with the potential to form an amphipathic α-helix. These features are generally found in other S100- and CaM-binding peptides (22) and are likely responsible for the faint binding of CaM.

The highly specific interaction of AHNAK repeat units with S100B provided a model target protein to evaluate the respective role of Ca^{2+} and Zn^{2+} binding to S100B. Previous studies using synthetic peptides corresponding to a calcium-sensitive epitope (TRTK-12) for S100B recognition revealed that although Zn^{2+} increases apparent peptide affinity for Ca^{2+}-S100B, Zn^{2+} is not directly implicated in binding of the target (37). In line with these observations, we found that Zn^{2+} binding alone to S100B is unable to promote AHNAK peptide binding. However, the binding of two Zn^{2+} equivalents to S100B enhances Ca^{2+}-dependent interactions (Fig. 9). In solution, S100B dimer is capable of binding up to 8 Zn^{2+}. The Zn^{2+} binding sites are not equivalent with respect to their affinity and associated conformational changes. Saturation of the two highest affinity Zn^{2+}-binding sites (K_d, 10–100 nM) has no significant effect on the overall S100B protein structure but produces drastic changes in Ca^{2+} binding affinity of site IIβ (10). In contrast, saturation of the lower affinity Zn^{2+}-binding sites on S100B produces drastic conformational changes, antagonizes calcium binding, and favors protein aggregation and precipitation. Thus, we consider it more likely that only the two high-affinity Zn^{2+}-binding sites on S100B may have regulatory functions. The three-dimensional structures of S100B and the related S100A7 predict that the highest affinity Zn^{2+}-binding site includes residues His^{85} and His^{90} (38, 39). These residues are located within the carboxyl-terminal domain that is essential for regulating Ca^{2+} binding to site IIβ (40). It is likely that Zn^{2+} binding to His^{85} and His^{90} induces subtle changes in the carboxyl-terminal region of S100B that increase accessibility of the EF-hand Ca^{2+} binding loop II to solvent (40). The increased affinity of Zn^{2+}-bound S100B for Ca^{2+} is illustrated by the shift to low calcium concentration of the Ca^{2+} titration curve for the interaction between Myc-tagged M1-DY AHNAK domains and S100B-Sepharose in the presence of Zn^{2+} (Fig. 9*B*). The Ca^{2+} titration curve in the presence of Zn^{2+} is in agreement with the binding affinity between S100B and Ca^{2+} determined under the same experimental condition (10). The effect of Zn^{2+} on the S100B-AHNAK interaction is maximal with the addition of 2 Zn^{2+} equivalents/mol S100B and decreased at higher Zn^{2+}:S100B molar ratios (Fig. 9*C*), confirming the regulatory role of the highest affinity sites. We therefore propose that Zn^{2+} regulates the function of S100B by binding and thereby regulating Ca^{2+}-dependent interactions of S100B with target molecules.

AHNAK/desmoyokin was first identified as a neuroblast differentiation-associated nuclear phosphoprotein (27). AHNAK was localized primarily (but not exclusively) to the nucleus of HeLa cells and neuroblastoma cells (28). In contrast with the predominant nuclear localization of human AHNAK protein in nonepithelial cells, the protein is found mainly at the plasma membrane in epithelial cells and is abundant within the cytoplasm of melanoma cells (29–30). Recently, Nie *et al.* (41) reported that a fragment consisting of the carboxyl-terminal 1002 amino acids of AHNAK (C-DY) accumulates in the nucleus of COS-7 cells, whereas N-DY and M-DY fragments remain cytoplasmic. The carboxyl-terminal region of AHNAK contains several putative nuclear localization signals (27). It is also characterized by the presence of a typical consensus leucine zipper sequence L-*X*(6)-L-*X*(6)-L-*X*(6)-L (residues 5012–5034) found in many gene-regulatory proteins (42). These

purified His-tagged M3-DY, U2-DY, and U1-DY AHNAK peptides used in *A, B,* and *C*. *B,* concentration dependence of the interaction of S100B with U2-DY peptide. Increasing concentrations of $2Zn^{2+}$-bound S100B as indicated were injected in running buffer on the sensor surface coated with U2-DY peptide. The interaction of S100B (140 nM) with U2-DY immobilized on the sensor chip surface is compared with S100A1, S100A6, S100A11, and calmodulin (140 nM each). Running buffer contains 20 mM Tris-HCl, pH 7.5, 150 mM NaCl, and 0.1 mM $CaCl_2$. The different sensorgrams shown here were obtained on the same sensor surface. *Inset* shows SDS-PAGE and Coomassie Blue staining of the purified human recombinant S100B, S100A1, S100A6, S100A11, and bovine brain calmodulin used in these studies. *C,* interaction of S100B with U1-DY peptide. U1-DY peptide was covalently immobilized on the sensor surface. S100B/Zn^{2+}(1:2 molar ratio), at the indicated concentration, was injected onto the sensor chip in running buffer containing 0.1 mM Ca^{2+}. After injection, the sensor chip was washed with calcium-containing running buffer. His-tagged importin α1 covalently immobilized on the sensor surface was used as a control. The *inset* shows binding of U1-DY AHNAK peptides (*Total*) to S100B-Sepharose beads in Ca^{2+}/Zn^{2+}-containing buffer (*Ca^{2+} / Zn^{2+}*) but not in EDTA/EGTA-containing buffer (*EDTA*).

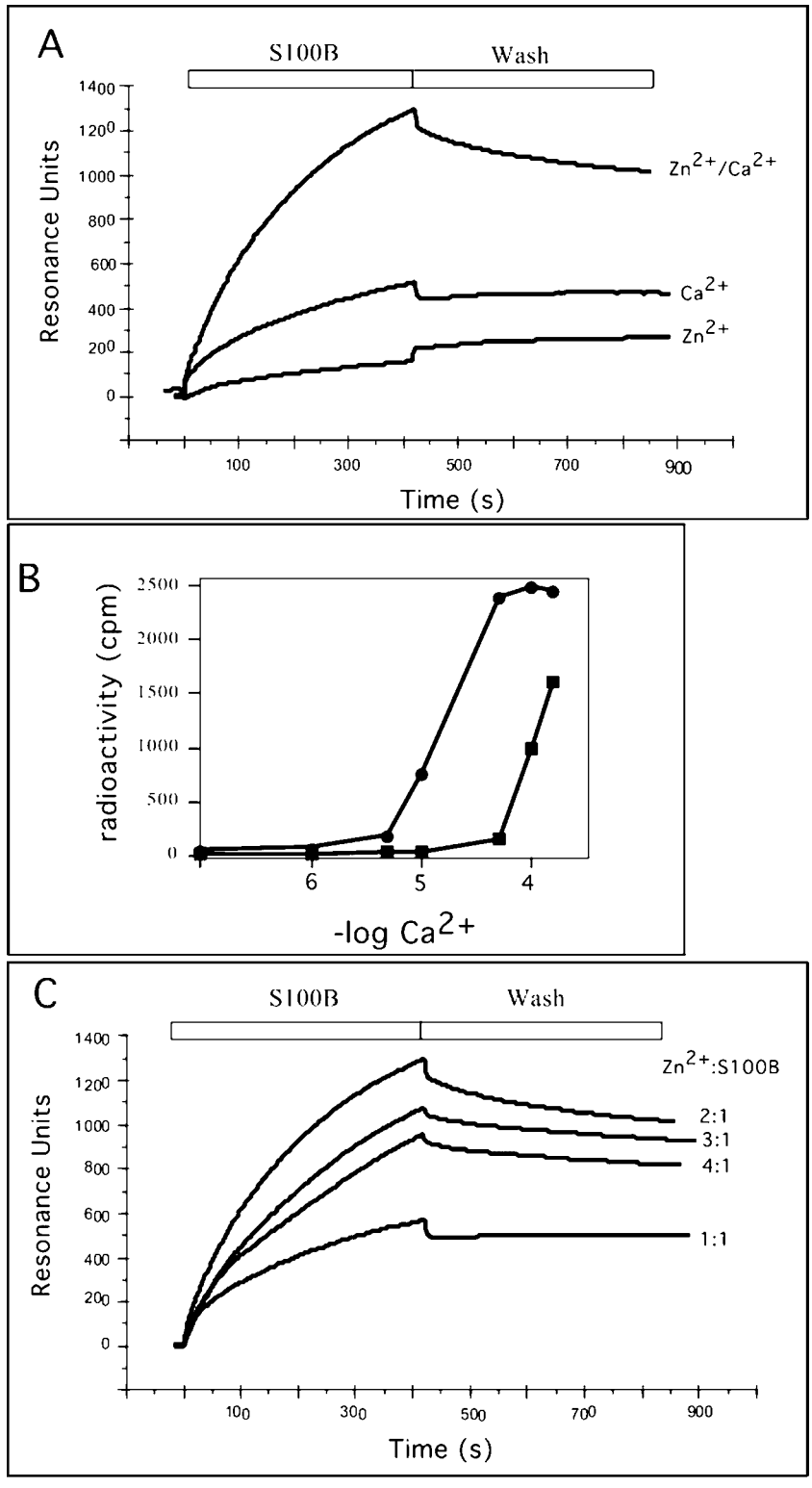

FIG. 9. **Zn^{2+} regulates S100B binding to AHNAK peptides.** *A,* Ca^{2+}- and Zn^{2+}-dependent interaction of S100B with U2-DY peptide. Recombinant human S100B (140 nM) in the presence of Ca^{2+} (0.1 mM) or Zn^{2+} (280 nM) or a mixture of Ca^{2+} and Zn^{2+} (0.1 mM Ca^{2+} and 280 nM Zn^{2+}), as indicated, was injected on U2-DY peptide immobilized on the sensor chip surface. At the end of the injection, the sensor surface was washed with running buffer (20 mM Tris-HCl, pH 7.5, 150 mM NaCl, and 0.1 mM $CaCl_2$). *B,* Ca^{2+} titration of the interaction of ^{35}S-labeled M1-DY domain expressed in rabbit reticulocyte with S100B-Sepharose. Interactions were studied in binding buffer in the absence (■) or presence of 10 μM $ZnSO_4$ (●). *C,* Zn^{2+} titration of the interaction between S100B with U2-DY peptide. Recombinant human S100B (140 nM) in the presence of various Zn^{2+}:S100B molar ratios, as indicated, was injected on U2-DY peptide immobilized on the sensor chip surface. At the end of the injection, sensor surface was washed with running buffer (20 mM Tris-HCl, pH 7.5, 150 mM NaCl, and 0.1 mM $CaCl_2$).

structural features suggest that the carboxyl-terminal region of AHNAK could have specialized nuclear functions. The dual intracellular location of AHNAK suggests the involvement of AHNAK in signal transduction pathways between the plasma membrane and the cell nucleus. A major feature of AHNAK is the repetitive heptad structure found in multiple copies within the large internal domain and the carboxyl terminus. The architectural arrangement of these repeat units in the full-length protein probably provides a scaffolding function that allows the assembly of multiprotein complexes. The strict calcium dependence of the interaction between S100B and repeat units on AHNAK indicates that AHNAK is probably not a S100B anchor protein but most likely a protein subjected to regulation by calcium and S100B. In the cytoplasm, a possible function for S100B could be to regulate AHNAK interaction with other cellular proteins. Such a model is supported by the observation that S100B is capable of preventing co-immunoprecipitation of AHNAK with the $p53val^{135}$ in REF clone 6 cell extracts (Fig. 1). In REF clone 6 cells, $p53val^{135}$ is sequestered in the cytoplasm by an as yet unidentified short-lived protein (43). Within the cytoplasm, $p53val^{135}$ cooperates with ras for cell transformation (44). AHNAK could be part of a cytoplasmic

scaffold protein complex involved in p53val^{135} cytoplasmic sequestration. In support of this, we have found that in REF cells, AHNAK is a short-lived cytoplasmic protein and that cycloheximide-mediated p53val^{135} nuclear accumulation (43) correlates with AHNAK protein degradation (data not shown). Alternatively, the interaction of AHNAK with p53val^{135} could be associated with the transforming activity of this p53 mutant protein (45). Dissociation of protein complexes involving p53val^{135} and AHNAK by S100B might explain the effect of S100B on both reversion of the transformed phenotype of clone 6 cells (33) and the nuclear accumulation of the p53val^{135} protein (34). The exact functional relationship between AHNAK and p53 proteins is under investigation.

The interaction of S100B with AHNAK might also open new opportunities for understanding the role played by S100B in the regulation of Ca^{2+} homeostasis within cells. Astrocytes derived from S100B null mice exhibit enhanced Ca^{2+} flux in response to depolarization or caffeine, suggesting that S100B plays a role in the maintenance of Ca^{2+} homeostasis in astrocytes through regulation of intracellular calcium flux (18). AHNAK has recently been found to be associated with a protein complex containing the β2 subunit of L-type calcium channel (31). S100B may thus represent a regulator protein for AHNAK L-type calcium channel interaction in astrocytes. It is also significant that S100B is up-regulated in rat and human cardiomyocytes after ischemic injury and acts as a negative modulator of the adrenergic-mediated hypertrophic response (16–17). In cardiomyocytes, AHNAK is thought to play a role in cardiac adrenergic signal transduction (31). S100B-dependent regulation of AHNAK in the adrenergic-mediated hypertrophic response should clearly now be investigated. S100B might also represent a possible regulator protein for other functions of AHNAK within cells. AHNAK has recently been characterized as a protein that binds and activates phospholipase C-γ. The repeated motifs on AHNAK are directly implicated in phospholipase C-γ activation (32). Activation of phospholipase C-γ by repeated AHNAK motifs triggers inositol 1,4,5-trisphosphate synthesis. Inositol 1,4,5-trisphosphate, through binding to its receptors, is directly implicated in Ca^{2+} release from intracellular calcium stores. Hence, through interaction with L-type calcium channels or phospholipase C-γ, AHNAK appears to be a protein that may play a key regulator function in calcium homeostasis regulation. We propose that S100B represents one AHNAK regulatory protein and that AHNAK regulation by S100B might provide a clue for understanding Ca^{2+} homeostasis regulation by S100B (18).

Acknowledgments—We thank Dr T. Hashimoto and Z. Nie for supplying Myc-tagged N-DY, M1-DY, and C-DY plasmids and for communicating their results before publication, Dr. E. Shtivelman for supplying KIS/AHNAK antibodies and AHNAK cDNA, Dr. M. Takahashi for providing us with monoclonal anti-S100B antibodies, Dr. H. Wientraub for MyoD antibody, and Dr. J. Lammarre for critical reading of the manuscript.

REFERENCES

1. Dolmetsch, R. E., Lewis, R. S., Goodnow, C. C., and Healy, J. I. (1997) *Nature* **286,** 855–858
2. McConkey, D. J., and Orrenius, S. (1994) *Trends Cell Biol.* **4,** 370–375
3. Nakayama, S., and Kretsinger, R. H. (1994) *Annu. Rev. Biophys. Biomol. Struct.* **23,** 473–507
4. Schäfer, B. W., and Heizmann, C. (1996) *Trends Biochem. Sci.* **21,** 134–140
5. Tarabykina, S., Kriajevska, M., Scott, D. J., Hill, T. J., Lafitte, D., Derrick, P. J., Dodson, G. G., Lukanidin, E., and Bronstein, I. (2000) *FEBS Lett.* **475,** 187–191
6. Wang, G., Rudland, P. S., White, M. R., and Barraclough, R. (2000) *J. Biol. Chem.* **275,** 11141–11146
7. Yang, Q., O'Hanlon, D., Heizmann, C. W., and Marks, A. (1999) *Exp. Cell Res.* **246,** 501–509
8. Deloulme, J. C., Assard, N., Ouengue Mbele, G., Mangin, C., Kuwano, R., and Baudier, J. (2000) *J. Biol. Chem.* **275,** 35302–35310
9. Schafer, B. W., Fritschy, J. M., Murmann, P., Troxler, H., Durussel, I., Heizmann, C. W., and Cox, J. A. (2000) *J. Biol. Chem.* **275,** 30623–30630
10. Baudier, J., Glasser, N., and Gérard, D. (1986) *J. Biol. Chem.* **261,** 8192–8203
11. Allore, R., O'Hanlon, D., Price, R., Neilson, K., Willard, H. F., Cox, D. R., Marks, A., and Dunn, R. J. (1988) *Science* **239,** 1311–1313
12. Griffin, W. S. T., Stanley, L. C., Ling, C., White, L., MacLeod, V., Perrot, L. J., White, C. L., and Araoz, C. (1989) *Proc. Natl. Acad. Sci. U. S. A.* **86,** 7611–7615
13. Sheng, J. G., Mrak, R. E., and Griffin, W. S. T. (1994) *J. Neurosci. Res.* **39,** 398–404
14. Stanley, L. C., Mrak, R. E., Woody, R. C., Perrot, L. J., Zhang, S., Marshak, D. R., Nelson, S. J., and Griffin, W. S. (1994) *J. Neuropathol. Exp. Neurol.* **53,** 231–238
15. Cochran, A. J., Lu, H. F., Li, P. X., Saxton, R., and Wen, D. R. (1983) *Melanoma Res.* **3,** 325–330
16. Tsoporis, J. N., Marks, A., Kahn, H. J., Butany, J., Liu, P. P., O'Hanlon, D., and Parker, T. G. (1997) *J. Biol. Chem.* **272,** 31915–31921
17. Tsoporis, J. N., Marks, A., Kahn, H. J., Butany, J., Liu, P. P., O'Hanlon, D., and Parker, T. G. (1998) *J. Clin. Invest.* **102,** 1609–1616
18. Xiong, Z., O'Hanlon, D., Becker, L. E., Roder, J., MacDonald, J. F., and Marks, A. (2000) *Exp. Cell Res.* **257,** 281–289
19. Baudier, J., and Cole, R. D. (1988) *J. Biol. Chem.* **263,** 5876–5883
20. Fujii, T., Mashino, K., Andoh, H., Satoh, T., and Kondo, Y. (1990) *J. Biochem. (Tokyo)* **107,** 133–137
21. Ivanenkov, V. V., Jamieson, G. A., Gruenstein, E., and Dimlich, R. V. W. (1995) *J. Biol. Chem.* **270,** 14651–14658
22. Millward, T. A., Heizmann, C. W., Schäfer, B. W., and Hemmings, B. A. (1998) *EMBO J.* **17,** 5913–5922
23. Zimmer, D. B, and Van Eldik, L. J. (1986) *J. Biol. Chem.* **261,** 11424–11428
24. Pozdnyakov, N., Goraczniak, R., Margulis, A., Duda, T., Sharma, R. K., Yoshida, A., and Sitaramayya, A. (1997) *Biochemistry* **36,** 14159–14166
25. Baudier, J., Bergeret, E., Bertacchi, N., Weintraub, H., Gagnon, J., and Garin, J. (1995) *Biochemistry* **34,** 7834–7846
26. Delphin, C., Ronjat, M., Deloulme, J. C., Garin, G., Debussche, L., Higashimoto, Y., Sakaguchi, K., and Baudier, J. (1999) *J. Biol. Chem.* **274,** 10539–10544
27. Shtivelman, E., Cohen, F. E., and Bishop, M. J. (1992) *Proc. Natl. Acad. Sci. U. S. A.* **89,** 5472–5476
28. Shtivelman, E., and Bishop, M. J. (1993) *J. Cell Biol.* **120,** 625–630
29. Hashimoto, T., Amagai, M., Parry, D. A., Dixon, T. W., Tsukita, S., Tsukita, S., Miki, K., Sakai, K., Inokuchi, Y., Kudoh, J., Shimizu, N., and Nishikawa, T. (1993) *J. Cell Sci.* **105,** 275–286
30. Hashimoto, T., Gamou, S., Shimizu, N., Kitajima, Y., and Nishikawa, T. (1995) *Exp. Cell Res.* **217,** 258–266
31. Haase, H., Podzuweit, T., Lutsch, G., Hohaus, A., Kostka, S., Lindschau, C., Kott, M., Kraft, R., and Morano, I. (1999) *FASEB J.* **13,** 2161–2172
32. Sekiya, F., Bae, Y. S., Jhon, D. Y., Hwang, S. C., and Rhee, S. G. (1999) *J. Biol. Chem.* **274,** 13900–13907
33. Scotto, C., Deloulme, J. C., Rousseau, D., Chambaz, E., and Baudier, J. (1998) *Mol. Cell. Biol.* **18,** 4272–4281
34. Scotto, C., Delphin, C., Deloulme, J. C., and Baudier, J. (1999) *Mol. Cell. Biol.* **19,** 7168–7180
35. Marshak, D. R., Watterson, D. M., and Van Eldik, L. J. (1981) *Proc. Natl. Acad. Sci. U. S. A.* **11,** 6793–6797
36. Heierhorst, J., Mann, R. J., and Kemp, B. E. (1997) *Eur. J. Biochem.* **249,** 127–133
37. Barber, K. R., McClintock, K. A., Jamieson, G. A., Dimlich, R. V. W., and Shaw, G. S. (1999) *J. Biol. Chem.* **274,** 1502–1508
38. Mäler, L., Potts, B. C. M., and Chazin, W. J. (1999) *J. Biomol. NMR* **13,** 233–247
39. Brodersen, D. E., Nyborg, J., and Kjeldgaard, M. (1999) *Biochemistry* **38,** 1695–1704
40. Baudier, J., Glasser, N., and Duportail, G. (1986) *Biochemistry* **25,** 6934–6941
41. Nie, Z., Ning, W., Amagai, M., and Hashimoto, T. (2000) *J. Invest. Dermatol.* **114,** 1044–1049
42. Busch, S. J., and Sassone-Corsi, P. (1990) *Trends Genet.* **6,** 36–40
43. Gannon, J. V., and Lane, D. P. (1991) *Nature* **349,** 802–805
44. Michalovitz, D., Halevy, O., and Oren, M. (1990) *Cell* **62,** 671–680
45. Shaulian, E., Zauberman, A., Ginsberg, D., and Oren, M. (1992) *Mol. Cell. Biol.* **12,** 5581–5592